Publ. Astron. Soc. Japan (2020) 72 (4), L7 (1–6)
doi: 10.1093/pasj/psaa055
Advance Access Publication Date: 2020 June 18
Letter

Letter

Probing cosmic rays with Fe Kα line structures generated by multiple ionization process

Hiromichi Okon,[1,*] Makoto Imai,[2] Takaaki Tanaka,[1] Hiroyuki Uchida,[1] and Takeshi Go Tsuru[1]

[1]Department of Physics, Kyoto University, Kitashirakawa-oiwake-cho, Sakyo-ku, Kyoto, Kyoto 606-8502, Japan
[2]Department of Nuclear Engineering, Kyoto University, Katsura, Nishikyo-ku, Kyoto, Kyoto 615-8540, Japan

*E-mail: okon@cr.scphys.kyoto-u.ac.jp

Received 2020 April 9; Accepted 2020 May 17

Abstract

Supernova remnants (SNRs) have been regarded as major acceleration sites of Galactic cosmic rays. Recent X-ray studies revealed neutral Fe Kα line emission from dense gas in the vicinity of some SNRs, which can be best interpreted as K-shell ionization of Fe atoms in the gas by sub-relativistic particles accelerated in the SNRs. In this Letter, we propose a novel method of constraining the composition of particles accelerated in SNRs, which is currently unknown. When energetic heavy ions collide with target atoms, their strong Coulomb field can easily cause simultaneous ejection of multiple inner-shell electrons of the target. This results in shifts in characteristic X-ray line energies, forming distinctive spectral structures. Detection of such structures in the neutral Fe Kα line strongly supports the particle ionization scenario, and furthermore provides direct evidence of heavy ions in the accelerated particles. We construct a model for the Fe Kα line structures by various projectile ions utilizing atomic-collision data.

Key words: atomic processes — cosmic rays — ISM: supernova remnants — line: formation — radiation mechanisms: non-thermal

1 Introduction

Supernova remnants (SNRs) have been regarded as major acceleration sites of Galactic cosmic rays (CRs). Radio, X-ray, and gamma-ray observations have been providing evidence that particles are indeed accelerated in expanding shells of SNRs via the diffusive shock acceleration mechanism (e.g., Koyama et al. 1995; Aharonian et al. 2007; Ackermann et al. 2013). However, the emission channels detected are all radiations from relativistic particles, and thus particles with lower energies were almost unexplored until recently.

Suzaku data recently revealed the presence of enhanced neutral Fe Kα (∼6.4 keV) line emission in some SNRs, where gamma-rays are detected and thus particle acceleration is expected to be at work (e.g., W 44: Nobukawa et al. 2018; W 28: Okon et al. 2018; G323.7−1.0: Saji et al. 2018). In most cases, the line emission spatially coincides with dense gas in the vicinity of the SNRs. Based on these results, the authors interpreted that the Fe line emission is due to K-shell ionization of Fe atoms in the gas by particles accelerated in the SNRs. If this interpretation is the case, sub-relativistic particles are mainly responsible for the

Fe emission line since the production cross-sections of the line emission peak at ∼10 MeV and ∼20 keV for protons and electrons, respectively (Dogiel et al. 2011).

Information on accelerated sub-relativistic particles can be exploited using the neutral Fe line emission. Dogiel et al. (2011) proposed an idea that species of radiating particles can be distinguished based on the equivalent width of the Fe line with respect to a non-thermal bremsstrahlung continuum from the same population of particles. Using the idea, Nobukawa et al. (2018, 2019) and Saji et al. (2018) claimed that protons account for the majority of the Fe line emission in some SNRs. Makino et al. (2019) presented an analytical model in which they consider energy-dependent escape of CRs from an SNR shock into an interacting cloud, and calculated emission spectra from the cloud, i.e., Fe line emission from sub-relativistic protons and π^0-decay emission from relativistic protons. Applying their model to W 44 and W 28, they successfully reproduced both the observed Fe line emission intensity and the gamma-ray spectra.

Fine structures of the Fe Kα line, if detected, can provide another step forward in the study of sub-relativistic particles accelerated in astrophysical objects. Tatischeff et al. (2012) pointed out that charge exchange between fast heavy ions and ambient neutral atoms can produce broad line structures accompanied with narrower K-shell lines. Detection of such structures would allow us to prove the presence of heavy ions in accelerated particles and to constrain their composition. Apart from charge exchange, multiple ionization, which is the topic of this Letter, is another potentially important process caused by accelerated heavy ions, and thus can be a powerful diagnostic tool to probe accelerated particles.

In the present work, we qualitatively estimate the effect of the multiple ionization process on the Fe Kα line emission. We calculate a model to predict line structures due to multiple ionization by using the knowledge from beam experiments. Based on our model, we show Fe Kα line structures expected to be detected in SNRs by high-resolution X-ray spectroscopy with X-Ray Imaging and Spectroscopy Mission (XRISM).

2 Kα line structures by impacts of mono-energetic ions

2.1 KαL^i peaks due to multiple ionization process

Ionization process of target atoms by projectile ions have been widely studied through both experimental and theoretical approaches. Through studies using high-resolution crystal spectrometers, authors such as Burch, Richard, and Blake (1971) and Kauffman et al. (1973) found differences of line structures between proton- and ion-produced Kα spectra. Figure 1 shows spectra of Fe Kα line structures originally presented by Burch, Richard, and Blake (1971). The proton-produced spectrum has only the neutral Fe Kα_1 and Fe Kα_2 lines due to the K–L$_1$ and K–L$_2$ transitions, respectively. The O^{5+}-produced spectrum, on the other hand, has broad line-like structures in the 6350–6550 eV band. When projectile particles are heavy ions, their strong Coulomb field can easily cause simultaneous ejection of multiple inner-shell electrons of targets, resulting in the significant characteristic structures.

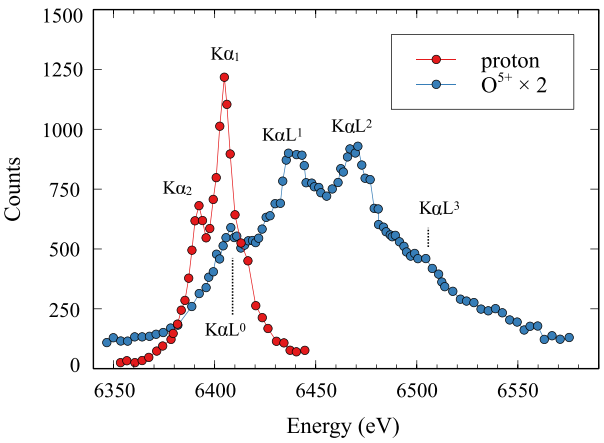

Fig. 1. Fe Kα spectra produced by impacts of protons (red), and O^{5+} ions (blue) (Burch et al. 1971). For display purposes, the O^{5+} spectrum is scaled by a factor of two. (Color online)

The multiple ionization structures consist of peaks called KαL^i ($i = 0$–7), each of which is a superposition of the K–L$_1$ and the K–L$_2$ transition lines from ionized Fe atoms with i L-shell vacancies. The center energies of the KαL^i peaks are higher by $\sim i \times$ 20–30 eV than those of the Fe Kα_1 and Kα_2 lines. This is because the K–L$_1$ (K–L$_2$) transition lines shift upwards by ∼20–30 eV per L-shell electron ionization ($=\Delta E_{\rm L}$) (e.g., Wang et al. 2012). The outer shell (M, N, ...) ionization is mainly manifested in broadenings of the KαL^i peaks because the energy shift $\Delta E_{\rm M}$ (and $\Delta E_{\rm N}$, ...) of the transition lines due to additional M-shell and outer shell vacancies is sufficiently smaller than $\Delta E_{\rm L}$, and is equal to or smaller than the natural widths of the transition lines.

2.2 Modeling of KαL^i peaks

The KαL^i peaks are the sums of the Kα_1L^i and Kα_2L^i sub-peaks, which are superpositions of the K–L$_1$ and K–L$_2$ transition lines, respectively. The Kα_1L^i (Kα_2L^i) sub-peaks are expressed as superpositions of Lorentzians corresponding to transition lines. According to Horvat, Watson, and Peng (2006, 2009), KαL^i spectra obtained in ion beam experiments can phenomenologically be reproduced by the sums of the Kα_1L^i and Kα_2L^i peaks described by Voigt functions, or a convolution of a Lorentzian and

a Gaussian. Here, the Gaussian reflects broadening of the sub-peaks due to simultaneous ionization of electrons in outer shells. Taking the same approach, we modeled the $K\alpha_1 L^i$ and $K\alpha_2 L^i$ sub-peaks with the Voigt function.

We calculate the center energy of the sub-peaks with the scaling law given by Horvat, Watson, and Peng (2006). They expressed the energy shift ΔE^i(eV) of each $K\alpha_1 L^i$ ($K\alpha_2 L^i$) sub-peak with respect to the neutral $K\alpha_1$ ($K\alpha_2$) line emission based on various data obtained by ion beam experiments. The energy shift ΔE^i can be described as

$$\Delta E^i = p_L^X\,[(i-1)(Z_2-a)+b] + i(c + d\,Z_2 + e\,i + f\,i\,Z_2)\,\mathrm{eV}, \quad (1)$$

where $a = 9.11$, $b = 14.3$, $c = -11.64$, $d = 1.493$, $e = 0.755$, $f = -0.0112$, and Z_2 is the atomic number of the target. The parameter p_L^X is the ionization probability per L-shell electron in K-shell ionization. We calculate the ionization probability p_L^X with the model by Horvat, Watson, and Peng (2006),

$$p_L^X = a'/[1 + (b'/X_2)^{c'}], \quad (2)$$

where $a' = 0.537$, $b' = 2.11$, and $c' = 2.02$. The parameter X_2 is a universal function derived by Sulik et al. (1987), and is described as

$$X_2 = 4V[G(V)]^{1/2} Z_1/(2v_1), \quad (3)$$

where v_1, Z_1, V, and $G(V)$ are the projectile velocity in atomic units, where is normalized to the Bohr velocity $2.18 \times 10^6\,\mathrm{m\,s^{-1}}$, the atomic number of the projectile, the ratio of v_1 to the average velocity of electrons in target atoms, and the Gryzinski Geometrical factor, respectively. We employ an analytical formula found in McGuire and Richard (1973) for $G(V)$.

We then calculate the widths of the sub-peaks. The scaling law by Horvat, Watson, and Peng (2006) approximates the widths of the Gaussian of the Voigt function as

$$\sigma^i = a\,i\,(b-i)(Z_2-c)\mathrm{eV}, \quad (4)$$

where $a = 0.0246$, $b = 9.86$, and $c = 10.40$. Following Horvat, Watson, and Peng (2006), we fix the line width of the Lorentzian component to the natural widths of the transition lines obtained by Campbell and Papp (2001).

The above scaling laws by Horvat, Watson, and Peng (2006) are derived from experimental data using a variety of solid targets with $Z_2 = 17$–32 and projectile ions with $Z_1 = 6$–83 at 2.5–25 MeV amu^{-1}. The data cover impacts by various ions with $\sim$10 MeV amu^{-1}, where the cross-sections for K-shell ionization of Fe atoms (Z_2) peak. We applied the scaling laws to the calculation of the Fe line structures generated by impacts of various ions in the 0.5–1000 MeV amu^{-1} region, where collision nature is well-described by the perturbation theory and the scaling laws of Horvat, Watson, and Peng (2006) can be considered valid.

The intensity of each $K\alpha_1 L^i$ ($K\alpha_2 L^i$) sub-peak can be expressed as a function of p_L^X. Under an assumption of independent L-shell electron ionization, a binomial distribution of

$$I_i = I_{\mathrm{tot}} \binom{8}{i} p_L^{Xi} \left(1 - p_L^X\right)^{8-i}, \quad (5)$$

where

$$I_{\mathrm{tot}} = \sum_i^8 I_i, \quad (6)$$

gives a good description of the relative intensities of the $K\alpha L^i$ peaks (Kauffman et al. 1973).

According to Horvat, Watson, and Peng (2009), intensities of the $K\alpha L^i$ peaks are changed depending on the phase of the target, whether it is gas or solid. Compared to the solid target case, the Fe $K\alpha L^i$ peaks become dominant with gaseous targets. Horvat, Watson, and Peng (2009) derived the scaling law of p_L^X similar to the equation (2) from atomic data of collisions between various ions at $\sim$10 MeV amu^{-1} and monoatomic Ar gas. The scaling law for gas is the same as equation (2), but with $a' = 0.856$, $b' = 2.94$, and $c' = 1.71$.

2.3 Results

In figure 2a, we plot the models for the $K\alpha$ line emitted by solid Fe bombarded by protons and fully ionized O and Fe ions. Figure 2b is the same but for gaseous Fe. The results clearly indicate that the intensities of the $K\alpha L^i$ peaks depends on the charge state and kinetic energy of the projectiles. The larger charge the projectile has, the more significant the $K\alpha L^i$ peaks become. This is naturally explained by a stronger Coulomb field of heavy ions. Regardless of the projectile species, the Fe $K\alpha L^i$ peaks are the most significant when the projectile kinetic energy is $\sim$1.6 MeV amu^{-1}. Electrons generally are ejected most efficiently when the projectile ion velocity matches the average velocity of electrons in orbit of an atom (Bohr 1948). Since the kinetic energy of $\sim$1.6 MeV amu^{-1} is translated into a projectile velocity close to that of Fe-L electrons, L-shell electrons are efficiently ionized around this energy.

2.4 Assumptions

Figure 3 shows a comparison between the computed models and experimental data by Horvat, Watson, and

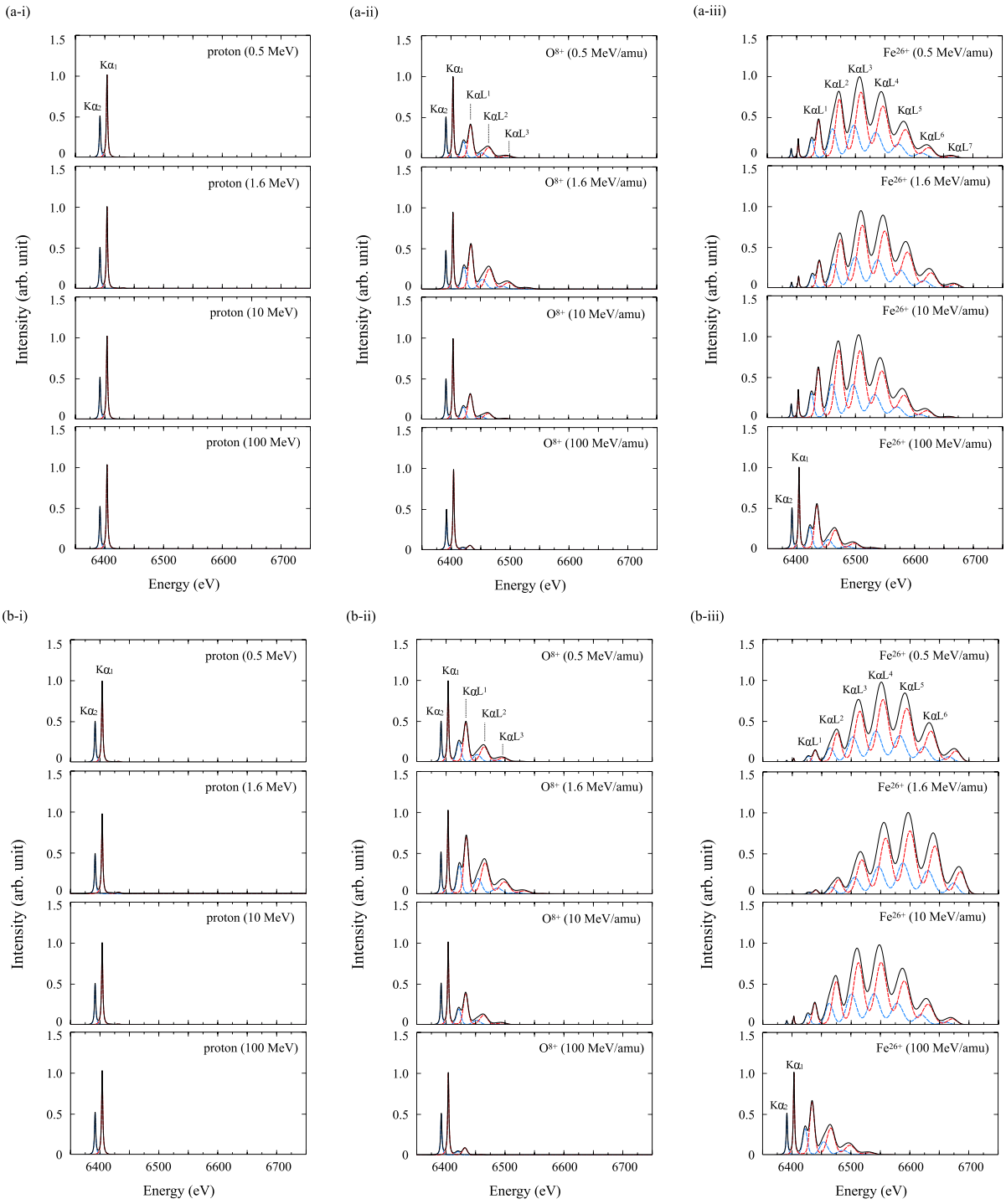

Fig. 2. Fe Kα structures emitted from (a) solid and (b) gaseous Fe targets under bombardment by (i) protons, (ii) O^{8+}, and (iii) Fe^{26+} ions. The red and blue dashed curves denote the Fe Kα_1 and Fe Kα_2 structures, respectively. (Color online)

Peng (2006, 2009). In the experimental data, the KαL^i peaks ($i = 0$–7) are generated by impacts of projectile ions, while the Kα_1 and Kα_2 lines in figure 3a are mainly induced by secondary electrons and X-rays. Our model reproduces the overall KαL^i peaks structures. However, we found some discrepancies of the line center energies and intensities. The contradiction about the center energy could be explained by the inaccuracy of equations (1), (2), and (4), which is estimated to be at a few percent level by Horvat, Watson, and Peng (2006). The discrepancy of the intensities could be brought about by continuous changes of energy and charge state of projectile ions in thick ($\sim$mg cm^{-2}) targets,

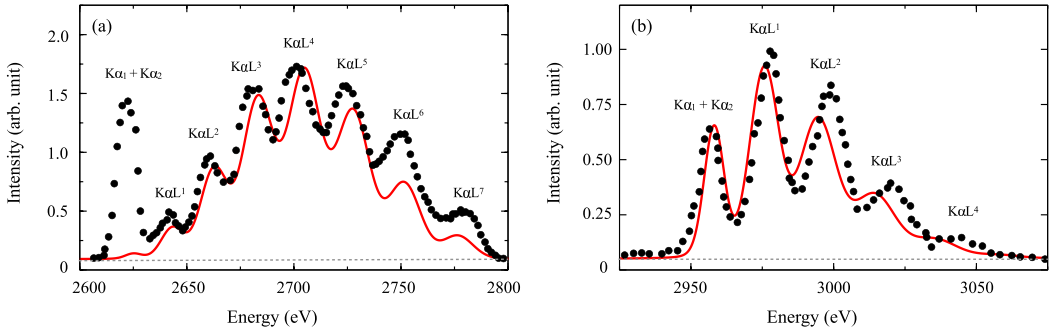

Fig. 3. (a) Cl Kα spectrum from solid KCl targets under bombardment by 4 MeV amu^{-1} Kr^{36+} ions (Horvat et al. 2006) and (b) Ar Kα spectrum from a gaseous Ar target under bombardment by 9.4 MeV amu^{-1} Ne^{10+} ions (Horvat et al. 2009) from experiments (the black dots), compared with our model (the red curves). The gray dashed curves represent the background. (Color online)

which change the value of p_L^X. Another possibility would be contribution of electron captures from the L-shell of the target atoms in L-shell vacancy production, as Rymuza et al. (1989) and Kavčič et al. (2000) pointed out. Those effects are not included in the present model.

3 Fe Kα structures produced by CRs

Using our model, we compute Fe Kα line spectra expected to be observed in SNRs. In SNR shocks, various ions would be accelerated at the same time, and thus the spectra would be superpositions of contributions from each ion species. Since the composition of CRs at acceleration sites is unknown, we here assume it is the same as that observed in the solar system by referring to Mewaldt (1994). We also assume that ions are fully ionized and that all ions follow a common spectrum. We take into account contributions from H, He, ..., Fe, Co, and Ni ions in an energy range of 0.5–1000 MeV amu^{-1}.

The flux of the Fe KαL^i peak F_i by each ion species can be described as

$$F_i \propto n_{\rm gas} \int \sigma_{{\rm KL}^i}\, v_{\rm ion}\, \frac{dN_{\rm ion}}{dE}\, dE, \tag{7}$$

where $n_{\rm gas}$, $\sigma_{{\rm KL}^i}$, $v_{\rm ion}$, and $dN_{\rm ion}/dE$ are the number density of Fe atoms in the dense gas, the production cross-section of the Fe KαL^i peak, the velocity of the ions, and the differential spectrum of the ion, respectively. We applied the scaling laws for solid targets assuming that Fe is mainly in dust grains. Based on equations (5) and (6), the production cross-section $\sigma_{{\rm KL}^i}$ can be calculated as

$$\sigma_{{\rm KL}^i} = \sigma_{\rm p} \binom{8}{i} p_L^{X^i} \left(1 - p_L^X\right)^{8-i}, \sigma_{\rm p} = \omega_{\rm K} \times \sigma_{\rm ion}, \tag{8}$$

where $\sigma_{\rm p}$, $\sigma_{\rm ion}$, and $\omega_{\rm K}$ are the production cross-section of the Fe Kα ($=\sum_i$ Fe KαL^i peaks) line, the K-shell ionization cross-section, and the florescence yield (=0.34) (Krause 1979), respectively. We computed $\sigma_{\rm ion}$ with the program by Batič, Pia, and Cipolla (2013) based on the ECPSSR (Energy-Loss Coulomb-Repulsion Perturbed-Stationary-State Relativistic) theory (Brandt & Lapicki 1981).

3.1 Results and future observations

Figure 4 presents the result, where the models are folded with the response of the X-ray micro-calorimeter Resolve (Ishisaki et al. 2018) aboard XRISM (Tashiro et al. 2018). Accelerated ions have a power-law spectrum $dN/dE \propto E^{-s}$ with $s = 1$ and $s = 2$ in the panels (a) and (b), respectively. The former is chosen referring to the measurement of non-thermal bremsstrahlung in W 49 B by Tanaka et al. (2018). The latter is the index expected in diffusive shock acceleration at a strong shock. In both cases, the KαL^i (i = 1–7) peaks appear in the 6420–6700 eV band. The intensities of each KαL^i peak strongly reflect the composition of the emitting particles. If particles accelerated in SNRs have a similar ion composition to CRs arriving at the solar system, the most significant peak is the KαL^1 peak, which can be resolved into Kα_1L^1 and Kα_2L^1 with Resolve. The intensities of the two sub-peaks are ~1/10 of those of Kα_1 and Kα_2. The Fe Kα_1L^1 and Kα_2L^1 sub-peaks are shifted by ~30 eV with respect to the Fe Kα_1 and Kα_2.

A ~eV energy resolution by X-ray micro-calorimeters would be necessary to resolve the structures. In addition to XRISM, future missions such as Athena (Barcons et al. 2017) and Super DIOS (Ohashi et al. 2018) with X-ray micro-calorimeters will able to detect the line structures. Such studies will play a complementary role to CR-ionization rate estimates based on H_3^+ absorption lines (e.g., Indriolo et al. 2010). We finally note that potential targets would not be limited to SNRs, considering the recent claims of contribution of CR-ionization to the neutral Fe K line in the Arches cluster region (Tatischeff

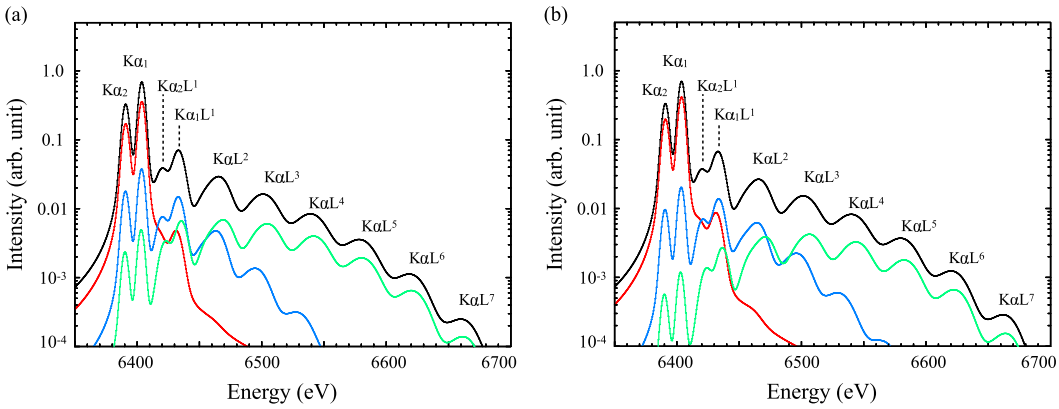

Fig. 4. Fe Kα structures expected from Fe atoms bombarded by accelerated particles with spectral indices of (a) $s = 1$ and (b) $s = 2$ (black). The red, blue, and green curves represent contributions from protons, O ions, and Fe ions, respectively. (Color online)

et al. 2012; Krivonos et al. 2017) and in the Galactic ridge (Nobukawa et al. 2015).

Acknowledgment

We thank T. Mukoyama, M. Pajek, B. Sulik, V. Tatischeff, and D. Banas for helpful discussion. This work is supported by JSPS/MEXT Scientific Research Grant Numbers JP19J14025 (H.O.), JP16K06937 (M.I.), JP19H01936 (T.T.), JP19K03915 (H.U.), and JP15H02090 (T.G.T.).

References

Ackermann, M., et al. 2013, Science, 339, 807
Aharonian, F., et al. 2007, A&A, 464, 235
Barcons, X., et al. 2017, Astron. Nachr., 338, 153
Batič, M., Pia, M. G., & Cipolla, S. J. 2013, Comput. Phys. Commun., 184, 2232
Bohr, N. 1948, Det Kgl. Danske Videnskabernes Selskab. Math.-fys. Medd. XVIII, No.8.
Brandt, W., & Lapicki, G. 1981, Phys. Rev. A, 23, 1717
Burch, D., Richard, P., & Blake, R. L. 1971, Phys. Rev. Lett., 26, 1355
Campbell, J. L., & Papp, T. 2001, Atomic Data Nucl. Data Tables, 77, 1
Dogiel, V., Chernyshov, D., Koyama, K., Nobukawa, M., & Cheng, K.-S. 2011, PASJ, 63, 535
Horvat, V., Watson, R. L., & Peng, Y. 2006, Phys. Rev. A, 74, 022718
Horvat, V., Watson, R. L., & Peng, Y. 2009, Phys. Rev. A, 79, 012708
Indriolo, N., Blake, G. A., Goto, M., Usuda, T., Oka, T., Geballe, T. R., Fields, B. D., & McCall, B. J. 2010, ApJ, 724, 1357
Ishisaki, Y., et al. 2018, J. Low Temperature Phys., 193, 991
Kauffman, R. L., McGuire, J. H., Richard, P., & Moore, C. F. 1973, Phys. Rev. A, 8, 1233
Kavčič, M., et al. 2000, Phys. Rev. A, 61, 052711
Koyama, K., Petre, R., Gotthelf, E. V., Hwang, U., Matsuura, M., Ozaki, M., & Holt, S. S. 1995, Nature, 378, 255
Krause, M. O. 1979, J. Phys. Chem. Ref. Data, 8, 307
Krivonos, R., et al. 2017, MNRAS, 468, 2822
McGuire, J. H., & Richard, P. 1973, Phys. Rev. A, 8, 1374
Makino, K., Fujita, Y., Nobukawa, K. K., Matsumoto, H., & Ohira, Y. 2019, PASJ, 71, 78
Mewaldt, R. A. 1994, Adv. Space Res., 14, 737
Nobukawa, K. K., et al. 2015, ApJ, 807, L10
Nobukawa, K. K., et al. 2018, ApJ, 854, 87
Nobukawa, K. K., Hirayama, A., Shimaguchi, A., Fujita, Y., Nobukawa, M., & Yamauchi, S. 2019, PASJ, 71, 115
Ohashi, T., et al. 2018, SPIE Proc., 10699, 1069928
Okon, H., Uchida, H., Tanaka, T., Matsumura, H., & Tsuru, T. G. 2018, PASJ, 70, 35
Rymuza, P., Sujkowski, Z., Carlen, M., Dousse, J.-C., Gasser, M., Kern, J., Perny, B., & Rhéme, C. 1989, Z. Phys. D Atoms Mol. Clusters, 14, 37
Saji, S., Matsumoto, H., Nobukawa, M., Nobukawa, K. K., Uchiyama, H., Yamauchi, S., & Koyama, K. 2018, PASJ, 70, 23
Sulik, B., Kádár, I., Ricz, S., Varga, D., Végh, J., Hock, G., & Berényi, D. 1987, Nucl. Instrum. Methods Phys. Res. B, 28, 509
Tanaka, T., et al. 2018, ApJ, 866, L26
Tashiro, M., et al. 2018, SPIE Proc., 10699, 1069922
Tatischeff, V., Decourchelle, A., & Maurin, G. 2012, A&A, 546, A88
Wang, X.-L., Dong, C.-Z., & Su, M.-G. 2012, Nucl. Instrum. Methods Phys. Res. B, 280, 93